

Enhanced phonon-drag by nanoscale design of homoepitaxial β -Ga₂O₃

Johannes Boy and Rüdiger Mitdank

Novel Materials Group, Humboldt-Universität zu Berlin, Newtonstraße 15, 12489 Berlin, Germany

Andreas Popp and Zbigniew Galazka

Leibniz-Institut für Kristallzüchtung, Max-Born-Strasse 2, 12489 Berlin, Germany

Saskia F. Fischer*

Novel Materials Group, Humboldt-Universität zu Berlin, Newtonstraße 15, 12489 Berlin, Germany and
Center for the Sciences of Materials, Humboldt-Universität zu Berlin, Zum Großen Windkanal 2, 12489 Berlin, Germany
(Dated: August 26, 2025)

Phonon drag may be harnessed for thermoelectric generators and devices. Here, we demonstrate the geometric control of the phonon-drag contribution to the thermopower. In nanometer-thin electrically conducting β -Ga₂O₃ films homoepitaxially-grown on insulating substrates it is enhanced from -0,4 mV/K to up to -3 mV/K at 100 K by choice of the film thickness. Analysis of the temperature-dependent Seebeck coefficients reveal that a crossover from three-dimensional to quasi-two-dimensional electron-phonon interaction occurs for film thicknesses below 75 nm. The ratio of phonon-phonon to electron-phonon relaxation times in these confined structures is 10 times larger than that of bulk. Generally the phonon drag can be tuned depending on the relations between the phonon-drag interaction length λ_{PD} , the phonon mean free path λ and the film thickness d . Phonon drag can be enhanced for $\lambda_{PD} \gg \lambda > d$.

Introduction– Phonon drag - the process whereby phonons drag along charge carriers - leads to a contribution to the thermopower in use for energy harvesting, thermoelectric generators and low-noise applications. The phonon drag depends on the phonon-phonon and electron-phonon interactions [1], and is influenced by the material choice, microstructure and defects [2–5]. Further, it is influenced by the mean-free path of charge carriers l_e and the dimensionality of the electrically conductive region [6, 7]. However, tailoring electron-phonon coupling by geometric control of homoepitaxial layers with *phonon-transparent* interfaces to the substrate [8] has not yet been elucidated.

Previous studies of phonon drag in confined structures have predominantly focused on heteroepitaxial structures. In a conducting film phonons drag charge carriers along by a transfer of momentum in-plane (Fig. 1 (a) and (b)). The phonon drag is determined by the material choices of film and substrate, whereby both, phonons and charges, are scattered at the interface [6, 9]. In particular, low-frequency acoustic phonons are effective contributors to the phonon drag because of their long lifetimes and, hence, long phonon mean free paths λ [2]. Phonon drag can be enhanced or decreased by confining the electrically conductive layer in polycrystalline [10] and heteroepitaxial layers [6, 9].

Homoepitaxial structures, instead, as depicted schematically in Fig. 1 (c) may allow ballistic phonon transport within the confined electrically conductive layers and through the homo-epitaxial, i.e. phonon-transparent, interface into the single crystalline substrate. This allows to decouple the cross sections of electron-phonon and phonon-phonon interactions. Hence, by geometrical design it is expected that the phonon drag can be tuned in homoepitaxially grown layers.

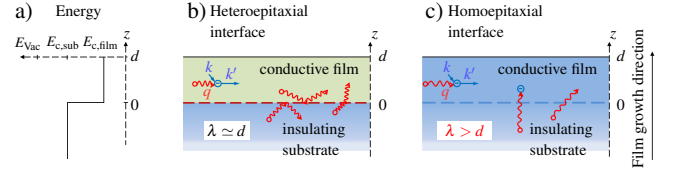


FIG. 1. (a) Schematic drawing of the conduction band edge E_c over film/substrate depth z . The electron mean free path is smaller than the film thickness $l_e < d$. (b) and (c) schematic drawing of the phonon-drag momentum transfer processes with phonons (q) and electrons (k, k') in (b) heteroepitaxial films and (c) homoepitaxial films (this work). For any heterointerface the phonon mean free path λ is reduced by boundary scattering of the phonons at the heterointerface, whereas high-quality homoepitaxial films provide phonon-transparent interfaces.

In this Letter, we demonstrate phonon-drag enhancement by nanoscale design of homoepitaxial thin electrically conducting films β -Ga₂O₃ with phonon-transparent interfaces to the insulating substrate. The temperature-dependent thermoelectrical transport properties are investigated as a function of decreasing thickness, d , of the conducting film. The thermodiffusive S_d and phonon-drag S_{PD} contributions to the measured Seebeck coefficient S are analyzed with respect to a crossover from three-dimensional to two-dimensional electron-phonon interaction. Electrically conducting thin homoepitaxial layers (by doping) are combined with a phononic reservoir of the insulating substrate (by compensation doping) barely limited by boundary scattering. The same order of doping density in the conducting layer and compensation doping density insulating substrate ensure equivalent impurity scattering for phonons.

Material: β -Ga₂O₃– Of the wide bandgap ($E_g = 4.85$ eV) semiconductor β -Ga₂O₃ homoepitaxial thin films and bulk

* contact author: sfischer@physik.hu-berlin.de

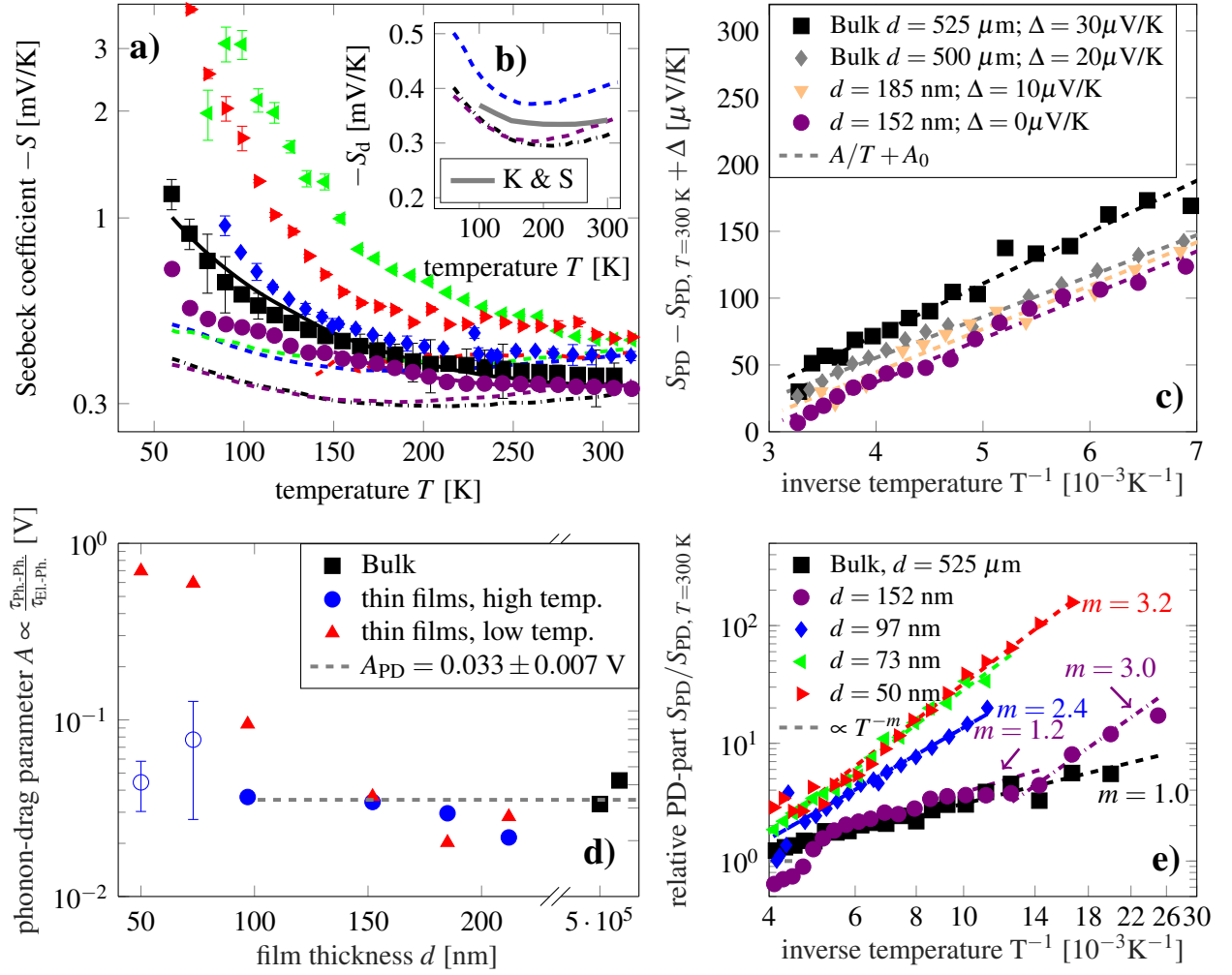


FIG. 2. (a) Experimental and theoretical Seebeck coefficient S and (b) thermodiffusion part of the Seebeck coefficient including values from Kumar and Singiseti [11] for β -Ga₂O₃ with an electron density of $n_{K\&S} = 5.5 \cdot 10^{17} \text{ cm}^{-3}$ as a function of temperature T for all β -Ga₂O₃ bulk and thin films with film thickness d . In (a) the thermodiffusion part (dashed line) for all samples and thermodiffusion plus phonon-drag part (solid) for the bulk sample is additionally shown. The thermodiffusion part is discussed in the Supplementary Information. The same legend as in (e) applies. (c) Relative Phonon-drag part and fit $S_{PD} = A/T + A_0$ as a function of inverse temperature for various bulk crystals and thick ($d \geq 150$ nm) films with offsets Δ for clarity. The $d = 185$ nm sample has been reported before [12]. (d) Phonon-drag parameter A as a function of film thickness d for various β -Ga₂O₃ bulk crystals and thin films for low ($T \leq 150$ K) and high ($T \geq 150$ K) temperatures. The high temperature regime of the thinnest films is well described by S_d , hence there is a major computational uncertainty for the high temperature phonon-drag part. The uncertainty of the solid symbols is smaller than the symbol size. (e) Phonon-drag part normalized to the room temperature value as a function of inverse temperature for various bulk crystals and films. The lines represent fits with $S_{PD} \propto T^{-m}$.

single crystals of high structural quality are available [13–20]. Room temperature mobilities of $\mu > 100 \text{ cm}^2/\text{Vs}$ and high power [21–23], optoelectronic [24] and gas sensing [25–27] device applications are reported. Previously, we determined the temperature-dependent electrical conductivity [28], thermal conductivity [29, 30] and Seebeck coefficient [12]. Foundational for this study, we reported on ballistic phonon transport through effectively phonon-transparent interfaces in high-quality homo-epi films [8], recently. In this work, Si-doped semiconducting homo-epi films on Mg-compensation doped insulating substrates both with doping densities in the same order of magnitude of $10^{17} - 10^{18} \text{ cm}^{-3}$ are used. Growth details, structural analysis and electrical characteri-

zation confirming the high quality of all samples are found in [31].

Transport parameters– The charge carrier density, mobility and Seebeck coefficient were determined for temperatures from 300 K to below 50 K [31]. The Hall-charge carrier density shows comparable doping for all samples ($n_{T=300 K} = 2.6 \cdot 10^{17}$ to $6.5 \cdot 10^{17} \text{ cm}^{-3}$) in magnitude and temperature dependence and reveals a donor level in the range of $E_{D1} = 18$ to 33 meV. The mobility is limited by polar optical phonons, neutral impurities and planar defects at high, intermediate and low temperatures, respectively. For very thin conducting epi-films $d \leq 73$ nm on insulating substrates the scattering on planar defects increases and dominates the entire tempera-

ture regime. The measured Seebeck coefficient S as a function of temperature is depicted in Fig. 2 (a) including the thermodiffusion part of the Seebeck coefficient determined from the reduced chemical potential and scattering parameter. The room temperature values for all samples are in the range $S_{T=300\text{ K}} = -330$ to $-460 \mu\text{V/K}$ and increase with decreasing temperatures. The variety of the room temperature values for $d \geq 73$ nm is due to different charge carrier concentrations. The higher Seebeck coefficient of the $d = 50$ nm epi-film is additionally caused by the increase of the scattering factor, see [31].

At cryogenic temperatures the Seebeck coefficient increases for all samples. However, for epi-films of lower thickness than 100 nm the Seebeck coefficient increases strongly with decreasing film thickness, see Fig. 2 (a). As will be detailed below, the phonon-drag is enhanced by the *geometric* confinement of charge carriers in the thin conducting epi-films, whereas phonons may travel quasi-ballistically without boundary scattering into the insulating substrate.

Thermoeffusion– First, the thermoeffusive part of the Seebeck coefficient is discussed. It is calculated from the reduced chemical potential and scattering parameter for the samples with the highest and lowest charge carrier density (Fig. 2 (b)). For comparison, the first-principle calculations by Kumar and Singiseti [11] calculated for $\beta\text{-Ga}_2\text{O}_3$ with an electron density of $n_{\text{K\&S}} = 5.5 \cdot 10^{17} \text{ cm}^{-3}$ are shown. The experimentally determined and calculated values are in agreement. The slight offsets between the different samples are due to differences in doping, which affects the reduced chemical potential and the thermoeffusion part depends on the reduced chemical potential η and the scattering factor r as detailed in [31]. However, the thermoeffusion part of the Seebeck coefficient only accounts for a small subset (-300 to $-500 \mu\text{V/K}$) of S at lower temperatures (Fig. 2 (b)).

Phonon drag– The increase in the Seebeck coefficient observed at low temperatures for all samples is attributed to the phonon-drag. A systematic dependence of the phonon drag S_{PD} as a function of thickness is found after subtraction of the thermoeffusion part S_d from the measured total Seebeck coefficient S . For homo-epi films of a thickness larger than 100 nm the values for the phonon drag part $S_{\text{PD}}(T)$ are independent of the film thickness d . For homo-epi films of thickness less than 100 nm the slope of the phonon drag part $S_{\text{PD}}(T)$ increases as described by Figs. 2 (e) and 3.

The observed phonon-drag increase is analysed in the following. Generally, the absolute value of the phonon drag contribution is limited by the phonon occupation at ultra-low temperatures and by phonon scattering at high temperatures. In between it exhibits a maximum value. In this study, the phonon drag is measured at temperatures above this maximum, where the phonon transport is mainly determined by Umklapp scattering and the phonon mean free path is given by $\lambda \propto T^{-1}$. Accordingly, in this temperature regime the phonon-drag contribution to the Seebeck coefficient is determined by $S_{\text{PD}} = A/T + A_0$ [1]. For the conducting bulk single crystal a fit including the thermoeffusion and phonon-drag contributions to the Seebeck coefficient agrees well with the measured data (black solid line in Fig. 2 (a)). Slight remaining dis-

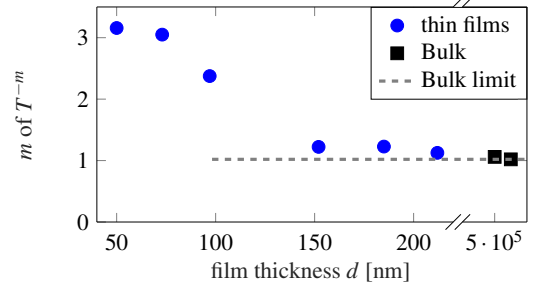


FIG. 3. Crossover from three-dimensional to two-dimensional electron-phonon interaction occurs for thin films, resulting in giant phonon-drag. Exponent m ($S_{\text{PD}} \propto T^{-m}$) as a function of film thickness d for various $\beta\text{-Ga}_2\text{O}_3$ bulk crystals and thin films. A steady increase of m with decreasing film thickness due to a change of phonon-transport in the thin film can be observed.

crepancies can be explained by computational uncertainties of reduced chemical potential η and scattering parameter r , and as well deviations from S_{PD} to the approximation given by $A/T + A_0$.

Fig. 2 (c) confirms for single crystal bulk and thick epi-films ($d \geq 150$ nm) that S_{PD} is proportional to the inverse temperature. Compared to the conducting bulk single crystal, the thick epi-films show a small decrease of the phonon-drag, which originates from the slight increase of phonon scattering in the epitaxial films, due to the silicon doping and lattice imperfections, which leads to a reduction of the phonon lifetime $\tau_{\text{Ph-Ph}}$. From the fit to the data with $S_{\text{PD}} = A/T + A_0$ for temperatures $T \geq 150$ K, a phonon-drag parameter $A = \text{const.} = (0.033 \pm 0.007) \text{ V}$ for bulk and thin films is determined.

A similar analysis for the thin films ($d \leq 100$ nm), however, separating the low ($T \leq 150$ K) and high ($T \geq 150$ K) temperature regimes, is depicted in Fig. 2 (d) and (e), respectively. A strong increase in the phonon-drag parameter occurs for film thicknesses below 75 nm, for $A = (0.69 \pm 0.02) \text{ V}$.

To understand the origin of the observed increase of S_{PD} for thin films, note that it relates to the phonon-phonon scattering time $\tau_{\text{Ph-Ph}}$ and the electron-phonon scattering time $\tau_{\text{El-Ph}}$ according to [1, 32, 33]

$$S_{\text{PD}} = -\frac{v^2}{T} \frac{1}{\mu_{\text{AP}}} \tau_{\text{Ph-Ph}} = \frac{m^* v^2}{eT} \cdot \frac{\tau_{\text{Ph-Ph}}}{\tau_{\text{El-Ph}}} \quad (1)$$

with μ_{AP} denoting the total electron mobility from scattering mechanisms transferring crystal momentum from acoustic phonons to electrons, v the sound velocity and m^* the effective mass. Here, low-frequency acoustic phonons are considered mainly responsible for the effective momentum transfer in the phonon-drag [1]. Thus, the phonon-drag parameter A directly depends on the ratio of the phonon-phonon to electron-phonon scattering times

$$a \cdot A = \frac{\tau_{\text{Ph-Ph}}}{\tau_{\text{El-Ph}}}, \quad (2)$$

with $a = e/(m^* v^2)$. This relates to the observation in Fig. 2 (d) that $A = T \cdot S_{\text{PD}} \propto \frac{\tau_{\text{Ph-Ph}}}{\tau_{\text{El-Ph}}}$ increases with decreasing film

thickness for low temperatures at which Umklapp scattering is reduced in the electrically conducting layer.

While both scattering times $\tau_{\text{Ph.-Ph.}}$ and $\tau_{\text{El.-Ph.}}$ increase with decreasing temperature due to a reduction of occupied phonon modes and the decrease of average phonon energy, however, the increase of A with decreasing film thickness d implies that the ratio of the scattering times is subject to the decreasing effective cross sectional area of the relevant momentum transfer for the phonon-drag.

The phonon-drag interaction length $\lambda_{\text{PD}} = v \cdot \tau_{\text{Ph.-Ph.}} = v \cdot a \cdot A \cdot \tau_{\text{El.-Ph.}}$ is directly proportional to the phonon-drag parameter A and the electron-phonon scattering time $\tau_{\text{El.-Ph.}}$. In a first approximation, the scattering times $\tau_{\text{El.-Ph.}}$ for 300 K and 100 K are about $9.4 \cdot 10^{-13}$ s and $4.8 \cdot 10^{-12}$ s, respectively. With $A = 0.033$ V and $a = 1.46 \cdot 10^4$ 1/V (with $m^* = 0.313 m_e$ and $v = 6200$ m/s) the value $a \cdot A \approx 500$ for bulk and thick films at 300 K and 100 K. However, for the thinnest films, the phonon-drag parameter strongly increases, leading to $a \cdot A \approx 10200$ at 100 K. Therefore, the phonon-drag interaction length increases from $\lambda_{\text{PD}}(100 \text{ K}) \approx 14 \mu\text{m}$ for bulk and thick films to $\lambda_{\text{PD, thin film}}(100 \text{ K}) \approx 300 \mu\text{m}$ for thin films. λ_{PD} thereby exceeds the phonon mean free path $\lambda(300 \text{ K}) \approx 3$ nm to $\lambda(100 \text{ K}) \approx 65$ nm by orders of magnitude [29]. This is due to the fact that the phonon drag is maximized if normal phonon scattering is dominant and decreases if Umklapp scattering occurs.

Generally, the electron-phonon coupling responsible for the phonon-drag occurs in all three dimensions in the bulk. However, in high-quality homoepitaxial films the relation between the film thickness d to the phonon mean free path (MFP) λ and the phonon-drag interaction length λ_{PD} may determine the magnitude of the phonon-drag. If the phonon mean free path exceeds the film thickness $\lambda > d$, the phonon-phonon Umklapp scattering in the electronically active region is reduced. Therefore, the low frequency phonons interact with the carriers undisturbed and hence, the phonon-drag contribution to the thermopower increases (Fig. 1 (c)). This in-plane momentum of the charge carriers is mainly dominant when the phonon mean free path λ describing the heat transfer exceeds the film thickness d . If $\lambda_{\text{PD}} \gg d > \lambda$, there is diffusive heat transport and the carriers can be scattered out of the plane by interaction with phonons. In the case of $\lambda_{\text{PD}} \gg \lambda > d$, the heat transfer vertical to the plane of the conducting layer is *quasi-ballistic*.

Phonon-phonon and electron-phonon interaction take place predominantly in-plane. Here, the condition $\lambda_{\text{PD}} \gg \lambda > d$ is fulfilled for $d < 100$ nm at 100 K, leading to an enhancement of the phonon-drag due to the crossover to quasi two-dimensional phonon transport. From Fauziah *et al.* [5] it is evident that the long wavelength phonons are responsible for the in-plane phonon drag. These phonons preferably propagate specularly. Furthermore, short wavelength phonons that contribute to the thermal conductivity by Umklapp scattering do not contribute to the phonon-drag. This means that local peculiarities with a diameter of the order of the surface roughness, such as lattice defects or impurities, are unessential for the interaction of electrons with phonons for the drag effect. In this study, the mean free path λ_{PD} exceeds by far the surface

roughness and therefore the specularly reflected lattice waves determine the phonon-drag. Therefore, S_{PD} coincides for thin films. This is contrary to S_d because there the interaction with boundary defects cannot be neglected.

Dimensionality of the relevant phonon transport– The observed dimensional crossover of the phonon drag with decreasing film thickness, is analysed to account for the nature of the phonon-phonon interaction and occupied phonon modes using [34, 35]

$$S_{\text{PD}} \propto T^{-7/2} \cdot T^{s/2+\gamma}. \quad (3)$$

For longitudinal acoustic phonons with the phonon wave-vector $q \rightarrow 0$ the exponent $s \rightarrow 0$ and $\gamma = 0$ and $\gamma = 2$ at low and high temperatures, respectively. For transversal acoustic phonons with $q \rightarrow 0$ the exponent $s \rightarrow -1$ and $\gamma = 0$ and $\gamma = 3$ at low and high temperatures, respectively. Using the experimental data, the resulting temperature dependence of the phonon-drag part normalized to the room temperature value is shown in Fig. 2 (e). For lower T the exponent m approximates to 3 (Fig. 2 (e)) if normal scattering dominates over Umklapp scattering. The total exponent $m = 7/2 - s/2 - \gamma$, as derived from eq. (3), is shown in Fig. 3 as a function of film thickness. A change of $\Delta m = 2$ between low and high temperature for longitudinal phonons occurs. From these results it follows that the bulk exhibits the temperature dependence $S_{\text{PD}} \propto T^{-m}$ with $m = 1$. This is expected because for bulk, in our case the thickness $d = 525 \mu\text{m} \gg \lambda(300 \text{ K}) \approx 3$ nm [29, 30] is much larger than the phonon mean free path. Thus, Umklapp processes are dominant [29, 30], which explain the observed $m = 1$. Lowering the temperature to $T = 100$ K the phonon mean free path increases to $\lambda \approx 65$ nm. Hence, only for the thickest films $d \geq 150$ nm will $m = 1$ for $T > 100$ K (Fig. 3).

For the thin films with $d \leq 100$ nm it is determined that $m \rightarrow 3$ for all temperatures. Here, λ is comparable to the thickness d of the epitaxial layers. This demonstrates a change of $\Delta m = 2$ induced by geometric confinement of the electrically conductive layer from $d > 150$ nm ($d > \lambda$) to $d \leq 100$ nm ($d < \lambda$).

Previously, the temperature induced change of the exponent $\Delta m = 2$ for bulk with $d \gg \lambda$ was discussed by Herring [34, 35] for germanium single crystals. In elastic anisotropic crystals the exponent m changes by $\Delta m = 2$ if the temperature is sufficiently low, because high-energy scattering processes like Umklapp scattering do not annihilate phonons. In this study, Fig. 3, $\Delta m = 2$ is induced by geometric confinement, which causes a reduced Umklapp scattering in the electrically conductive layer at low temperatures and enhances the phonon-drag contribution. This result of geometric confinement holds generally true if $\lambda > d$ and $\lambda_{\text{PD}} \gg d$ [10, 36] then the phonon drag can be enhanced [37, 38].

As shown, the phonon drag can be strongly enhanced by geometric confinement of conductive layer thickness below the phonon mean free path in homoepitaxial systems. The scattering cross sections of electron-phonon and phonon-phonon interactions can be tuned on the basis of phonon-transparent interfaces. The enhancement of the phonon-drag scales with the ratio of the phonon mean free path λ and the film

thickness d . For $\lambda/d \geq 1$ a quasi two-dimensional phonon transport takes place in-plane of the electrically conductive film. In the presented case the Seebeck coefficient at room temperature nearly doubles due to the reduced Umklapp scattering (see Fig. 2 (a)).

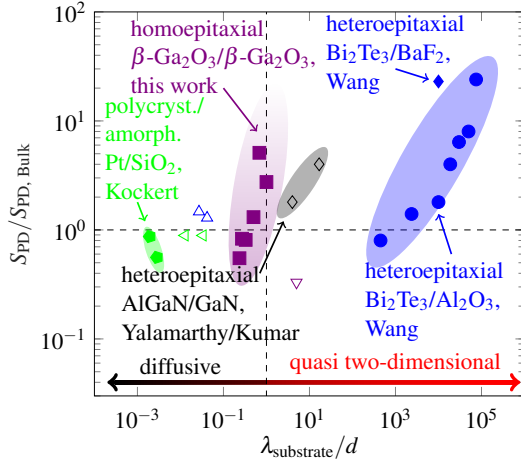


FIG. 4. Change of the phonon-drag part $S_{PD}/S_{PD, Bulk}$ over the ratio of the phonon mean free path of the substrate relative to the thickness of the electrically conductive material $\lambda_{\text{substrate}}/d$ for various quasi two-dimensional and quasi one-dimensional material systems. Shown is data for quasi two-dimensional systems of this work at $T = 100$ K (violet filled squares), epitaxial Bi_2Te_3 on BaF_2 at $T = 14$ K (blue filled diamond) and on Al_2O_3 at $T = 30$ K (blue filled circle) by Wang [9], sputtered and annealed Pt on SiO_2 at $T = 70$ K (green filled pentagons) by Kockert [10] and a two-dimensional electron gas in a $\text{AlGaIn}/\text{GaIn}$ heterostructure by Yalamarthy [6] compared to data from Kumar [39] at $T = 100$ K (black unfilled diamonds). Data for quasi one-dimensional systems are shown for Si-nanowires at $T = 100$ K (violet unfilled triangle pointing down) by Sadhu [38], Ag- (blue unfilled triangles pointing up) and Bi- (green unfilled triangles pointing left) nanowires by Kockert [36, 40] at $T = 75$ K and $T = 130$ K, respectively.

In Fig. 4 a summary of the variations reached by tuning

the phonon drag on behalf of geometrical confinement in various material systems including heteroepitaxial films ($\text{Bi}_2\text{Te}_3/\text{BaF}_2$ [9], $\text{Bi}_2\text{Te}_3/\text{Al}_2\text{O}_3$ [9], $\text{AlGaIn}/\text{GaIn}$ [6]). Evidently, for systems with heteroepitaxial interfaces a higher λ/d ratio is required to achieve the same increase of the phonon drag as for the homo-epi films from this study. In polycrystalline/amorphous metallic films of platinum on SiO_2 [10] heat flow is dominated by electrons in the metal layer. λ is very low in Pt and SiO_2 due to increased grain boundary scattering, lowering the phonon-drag. Finally, in nanowires [36, 38, 40], a reduction of λ due to boundary scattering on the surface of the nanowire was observed, which strongly reduces the phonon-drag effect.

Conclusion– Phonon-drag engineering may be utilized for low-temperature thermo-electrical applications. Phonon drag can be either maximized by reducing phonon Umklapp scattering, lattice mismatch and boundary scattering or minimized vice versa. Nanoscale design of homoepitaxial films allow to select diffusive or quasi-ballistic heat transfer: confinement of charge carriers combined with phonon-transparent interfaces may pave the way to adjust cross-sections of electrons with phonons to obtain the desired performance and function.

Data availability – The data that support the findings of this study are available from the corresponding authors upon request.

Acknowledgements – This work funded by the German Science Foundation (DFG FI932/10-2, DFG-FI932/10-1, DFG-FI932/11-1, WA 1453/3-1 and PO 2659/1-2) and was performed in the framework of GraFOx, a Leibniz-ScienceCampus partially funded by the Leibniz association. JB, RM and SFF are grateful for scientific and technical support by Dr. Olivio Chiatti.

Competing interests – The authors declare no competing interests.

[1] C. Herring, Theory of the thermoelectric power of semiconductors, *Physical Review* **96**, 1163 (1954).
[2] D. M. Rowe, ed., *Thermoelectrics Handbook: Macro to Nano* (CRC PR INC, 2005).
[3] H. Takahashi, R. Okazaki, S. Ishiwata, H. Taniguchi, A. Okutani, M. Hagiwara, and I. Terasaki, Colossal seebeck effect enhanced by quasi-ballistic phonons dragging massive electrons in FeSb_2 , *Nature Communications* **7**, 10.1038/ncomms12732 (2016).
[4] H. Matsuura, H. Maebashi, M. Ogata, and H. Fukuyama, Effect of phonon drag on seebeck coefficient based on linear response theory: Application to FeSb_2 , *Journal of the Physical Society of Japan* **88**, 074601 (2019).
[5] K. Fauziah, Y. Suzuki, T. Nogita, Y. Kamakura, T. Watanabe, F. Salleh, and H. Ikeda, Effect of phonon-boundary scattering

on phonon-drag factor in seebeck coefficient of Si wire, *AIP Advances* **10**, 075015 (2020).
[6] A. S. Yalamarthy, M. M. Rojo, A. Bruefach, D. Boone, K. M. Dowling, P. F. Satterthwaite, D. Goldhaber-Gordon, E. Pop, and D. G. Senesky, Significant phonon drag enables high power factor in the $\text{AlGaIn}/\text{GaIn}$ two-dimensional electron gas, *Nano Letters* **19**, 3770 (2019).
[7] I. Pallecchi, F. Telesio, D. Marré, S. G. D. Li, J.-M. Triscone, and A. Filippetti, Large phonon-drag enhancement induced by narrow quantum confinement at the $\text{LaAlO}_3/\text{SrTiO}_3$ interface, *PHYSICAL REVIEW B* **93**, 195309 (2016).
[8] R. Ahrling, R. Mitdank, A. Popp, J. Rehm, A. Akhtar, Z. Galazka, and S. F. Fischer, Resistive and ballistic phonon transport in $\beta\text{-Ga}_2\text{O}_3$, *Phys. Rev. B* **110**, 085302 (2024).
[9] G. Wang, L. Endicott, H. Chi, P. Lošćák, and C. Uher, Tun-

- ing the temperature domain of phonon drag in thin films by the choice of substrate, *Physical Review Letters* **111**, 10.1103/physrevlett.111.046803 (2013).
- [10] M. Kockert, R. Mitdank, A. Zykov, S. Kowarik, and S. F. Fischer, Absolute seebeck coefficient of thin platinum films, *Journal of Applied Physics* **126**, 105106 (2019).
- [11] A. Kumar and U. Singiseti, First principles study of thermoelectric properties of β -gallium oxide, *Applied Physics Letters* **117**, 262104 (2020).
- [12] J. Boy, M. Handweg, R. Ahrling, R. Mitdank, G. Wagner, Z. Galazka, and S. F. Fischer, Temperature dependence of the seebeck coefficient of epitaxial β -Ga₂O₃ thin films, *APL Materials* **7**, 022526 (2019).
- [13] Z. Galazka, R. Uecker, D. Klimm, K. Irmscher, M. Naumann, M. Pietsch, A. Kwasniewski, R. Bertram, S. Ganschow, and M. Bickermann, Scaling-up of bulk β -Ga₂O₃ single crystals by the czochralski method, *ECS Journal of Solid State Science and Technology* **6**, Q3007 (2016).
- [14] P. Mazzolini, P. Vogt, R. Schewski, C. Wouters, M. Albrecht, and O. Bierwagen, Faceting and metal-exchange catalysis in (010) β -Ga₂O₃ thin films homoepitaxially grown by plasma-assisted molecular beam epitaxy, *APL Materials* **7**, 022511 (2019).
- [15] Z. Cheng, M. Hanke, Z. Galazka, and A. Trampert, Growth mode evolution during (100)-oriented β -Ga₂O₃ homoepitaxy, *Nanotechnology* **29**, 395705 (2018).
- [16] R. Schewski, K. Lion, A. Fiedler, C. Wouters, A. Popp, S. V. Levchenko, T. Schulz, M. Schmidbauer, S. B. Anooz, R. Grüneberg, Z. Galazka, G. Wagner, K. Irmscher, M. Scheffler, C. Draxl, and M. Albrecht, Step-flow growth in homoepitaxy of β -Ga₂O₃ (100) - the influence of the miscut direction and faceting, *APL Materials* **7**, 022515 (2019).
- [17] S. B. Anooz, R. Grüneberg, C. Wouters, R. Schewski, M. Albrecht, A. Fiedler, K. Irmscher, Z. Galazka, W. Miller, G. Wagner, J. Schwarzkopf, and A. Popp, Step flow growth of β -Ga₂O₃ thin films on vicinal (100) β -Ga₂O₃ substrates grown by MOVPE, *Applied Physics Letters* **116**, 182106 (2020).
- [18] D. J. Comstock and J. W. Elam, Atomic layer deposition of Ga₂O₃ films using trimethylgallium and ozone, *Chemistry of Materials* **24**, 4011 (2012).
- [19] Z. Galazka, S. Ganschow, K. Irmscher, D. Klimm, M. Albrecht, R. Schewski, M. Pietsch, T. Schulz, A. Dittmar, A. Kwasniewski, R. Grueneberg, S. B. Anooz, A. Popp, U. Juda, I. M. Hanke, T. Schroeder, and M. Bickermann, Bulk single crystals of β -Ga₂O₃ and Ga-based spinels as ultra-wide bandgap transparent semiconducting oxides, *Progress in Crystal Growth and Characterization of Materials* **67**, 100511 (2021).
- [20] Z. Galazka, Gallium Oxide: Crystal Growth, Materials Properties, and Devices (Springer Nature Switzerland AG, 2020) Chap. Czochralski method, pp. 15 – 36.
- [21] M. Higashiwaki and G. H. Jessen, Guest editorial: The dawn of gallium oxide microelectronics, *Applied Physics Letters* **112**, 060401 (2018).
- [22] H. Zhou, K. Maize, G. Qiu, A. Shakouri, and P. D. Ye, β -Ga₂O₃ on insulator field-effect transistors with drain currents exceeding 1.5 A/mm and their self-heating effect, *Applied Physics Letters* **111**, 092102 (2017).
- [23] J. Yang, S. Ahn, F. Ren, S. J. Pearton, S. Jang, J. Kim, and A. Kuramata, High reverse breakdown voltage schottky rectifiers without edge termination on Ga₂O₃, *Applied Physics Letters* **110**, 192101 (2017).
- [24] Z. Galazka, β -Ga₂O₃ for wide-bandgap electronics and optoelectronics, *Semiconductor Science and Technology* **33**, 113001 (2018).
- [25] S. Manandhar, A. K. Battu, A. Devaraj, V. Shutthanandan, S. Thevuthasan, and C. V. Ramana, Rapid response high temperature oxygen sensor based on titanium doped gallium oxide, *Scientific Reports* **10**, 10.1038/s41598-019-54136-8 (2020).
- [26] A. Afzal, β -Ga₂O₃ nanowires and thin films for metal oxide semiconductor gas sensors: Sensing mechanisms and performance enhancement strategies, *Journal of Materiomics* **5**, 542 (2019).
- [27] Z. Liu, T. Yamazaki, Y. Shen, T. Kikuta, N. Nakatani, and Y. Li, O₂ and CO sensing of Ga₂O₃ multiple nanowire gas sensors, *Sensors and Actuators B: Chemical* **129**, 666 (2008).
- [28] R. Ahrling, J. Boy, M. Handweg, O. Chiatti, R. Mitdank, G. Wagner, Z. Galazka, and S. F. Fischer, Transport properties and finite size effects in β -Ga₂O₃ films, *Scientific Reports* **9**, 13149 (2019).
- [29] M. Handweg, R. Mitdank, Z. Galazka, and S. F. Fischer, Temperature-dependent thermal conductivity in Mg-doped and undoped β -Ga₂O₃ bulk crystals, *Semiconductor Science and Technology* **30**, 024006 (2015).
- [30] M. Handweg, R. Mitdank, Z. Galazka, and S. F. Fischer, Temperature-dependent thermal conductivity and diffusivity of a Mg-doped insulating β -Ga₂O₃ single crystal along [100], [010] and [001], *Semiconductor Science and Technology* **31**, 125006 (2016).
- [31] See supplemental material at url for crystal and homo-epitaxial film growth, experimental methods and electrical characterization results and evaluation procedures.
- [32] A. R. Hutson, Piezoelectric scattering and phonon drag in ZnO and CdS, *Journal of Applied Physics* **32**, 2287 (1961).
- [33] M. J. Smith and P. N. Butcher, Simple models of phonon-drag in 3D and quasi-2D, *Journal of Physics: Condensed Matter* **2**, 2375 (1990).
- [34] C. Herring, Halbleiter und phosphore / semiconductors and phosphors / semiconducteurs et phosphores (Vieweg+Teubner Verlag, 1958) Chap. The Role of Low-Frequency Phonons in Thermoelectricity and Thermal Conduction, pp. 184 – 235.
- [35] C. Herring, T. H. Geballe, and J. E. Kunzler, Phonon-drag thermomagnetic effects in *n*-type germanium. i. general survey, *Physical Review* **111**, 36 (1958).
- [36] M. Kockert, D. Kojda, R. Mitdank, A. Mogilatenko, Z. Wang, J. Ruhhammer, M. Kroener, P. Woias, and S. F. Fischer, Nanometrology: Absolute seebeck coefficient of individual silver nanowires, *Scientific Reports* **9**, 10.1038/s41598-019-56602-9 (2019).
- [37] E. B. Ramayya, L. N. Maurer, A. H. Davoody, and I. Knezevic, Thermoelectric properties of ultrathin silicon nanowires, *Physical Review B* **86**, 10.1103/physrevb.86.115328 (2012).
- [38] J. Sadhu, H. Tian, J. Ma, B. Azeredo, J. Kim, K. Balasundaram, C. Zhang, X. Li, P. M. Ferreira, and S. Sinha, Quenched phonon drag in silicon nanowires reveals significant effect in the bulk at room temperature, *Nano Letters* **15**, 3159 (2015).
- [39] A. Kumar, S. Singh, A. Patel, K. Asokan, and D. Kanjilal, Thermoelectric properties of GaN with carrier concentration modulation: an experimental and theoretical investigation, *Physical Chemistry Chemical Physics* **23**, 1601 (2021).
- [40] M. Kockert, R. Mitdank, H. Moon, J. Kim, A. Mogilatenko, S. H. Moosavi, M. Kroener, P. Woias, W. Lee, and S. F. Fischer, Semimetal to semiconductor transition in Bi/TiO₂ core/shell nanowires, *Nanoscale Advances* **3**, 263 (2021).
- [41] R. Stratton, Diffusion of hot and cold electrons in semiconductor barriers, *Physical Review* **126**, 2002 (1962).
- [42] N. G. Nilsson, An accurate approximation of the generalized einstein relation for degenerate semiconductors, *Physica Status Solidi (A)* **19**, K75 (1973).

- [43] T. Oishi, Y. Koga, K. Harada, and M. Kasu, High-mobility β -Ga₂O₃ (201) single crystals grown by edge-defined film-fed growth method and their schottky barrier diodes with ni contact, *Applied Physics Express* **8**, 031101 (2015).
- [44] K. Irmscher, Z. Galazka, M. Pietsch, R. Uecker, and R. Fornari, Electrical properties of β -Ga₂O₃ single crystals grown by the czochralski method, *Journal of Applied Physics* **110**, 063720 (2011).
- [45] A. T. Neal, S. Mou, S. Rafique, H. Zhao, E. Ahmadi, J. S. Speck, K. T. Stevens, J. D. Blevins, D. B. Thomson, N. Moser, K. D. Chabak, and G. H. Jessen, Donors and deep acceptors in β -Ga₂O₃, *Applied Physics Letters* **113**, 062101 (2018).
- [46] J. B. Varley, J. R. Weber, A. Janotti, and C. G. V. de Walle, Oxygen vacancies and donor impurities in β -Ga₂O₃, *Applied Physics Letters* **97**, 142106 (2010).
- [47] B. K. Ridley, *Quantum Processes in Semiconductors* (Oxford University Press, 2000).
- [48] Z. Guo, A. Verma, X. Wu, F. Sun, A. Hickman, T. Masui, A. Kuramata, M. Higashiwaki, D. Jena, and T. Luo, Anisotropic thermal conductivity in single crystal β -gallium oxide, *Applied Physics Letters* **106**, 111909 (2015).
- [49] A. Parisini and R. Fornari, Analysis of the scattering mechanisms controlling electron mobility in β -Ga₂O₃ crystals, *Semiconductor Science and Technology* **31**, 035023 (2016).
- [50] K. Seeger, *Semiconductor Physics*, 9th ed., edited by H. von Riedesel (Springer, 2004).
- [51] H. Brooks, *Advances in Electronics and Electron Physics*, edited by L. Marton, Vol. 7 (Academic Press, New York, 1955).
- [52] J. Y. W. Seto, The electrical properties of polycrystalline silicon films, *Journal of Applied Physics* **46**, 5247 (1975).
- [53] A. Fiedler, R. Schewski, M. Baldini, Z. Galazka, G. Wagner, M. Albrecht, and K. Irmscher, Influence of incoherent twin boundaries on the electrical properties of β -Ga₂O₃ layers homoepitaxially grown by metal-organic vapor phase epitaxy, *Journal of Applied Physics* **122**, 165701 (2017).
- [54] R. Schewski, M. Baldini, K. Irmscher, A. Fiedler, T. Markurt, B. Neuschulz, T. Remmele, T. Schulz, G. Wagner, Z. Galazka, and M. Albrecht, Evolution of planar defects during homoepitaxial growth of β -Ga₂O₃ layers on (100) substrates - a quantitative model, *Journal of Applied Physics* **120**, 225308 (2016).
- [55] A. Parisini, K. Ghosh, U. Singiseti, and R. Fornari, Assessment of phonon scattering-related mobility in β -Ga₂O₃, *Semiconductor Science and Technology* **33**, 105008 (2018).
- [56] J.-L. Farvacque, Extension of the collision-time tensor to the case of inelastic scattering mechanisms: application to GaAs and GaN, *Physical Review B* **62**, 2536 (2000).
- [57] J. Boy, M. Handweg, R. Mitdank, Z. Galazka, and S. F. Fischer, Charge carrier density, mobility, and seebeck coefficient of melt-grown bulk ZnGa₂O₄ single crystals, *AIP Advances* **10**, 055005 (2020).
- [58] Z. Galazka, K. Irmscher, R. Uecker, R. Bertram, M. Pietsch, A. Kwasniewski, M. Naumann, T. Schulz, R. Schewski, D. Klimm, and M. Bickermann, On the bulk β -Ga₂O₃ single crystal grown by the czochralski method, *Journal of Crystal Growth* **404**, 184 (2014).
- [59] Z. Galazka, R. Uecker, K. Irmscher, M. Albrecht, D. Klimm, M. Pietsch, M. Brützm, R. Bertram, S. Ganschow, and R. Fornari, Czochralski growth and characterization of β -Ga₂O₃ single crystals, *Crystal Research and Technology* **45**, 1229 (2010).
- [60] S. B. Anooz, A. Popp, R. Grüneberg, C. Wouters, R. Schewski, M. Schmidbauer, M. Albrecht, A. Fiedler, M. Ramsteiner, D. Klimm, K. Irmscher, Z. Galazka, and G. Wagner, Indium incorporation in homoepitaxial β -Ga₂O₃ thin films grown by metal organic vapor phase epitaxy, *Journal of Applied Physics* **125**, 195702 (2019).
- [61] S. B. Anooz, R. Grüneberg, T.-S. Chou, A. Fiedler, K. Irmscher, C. Wouters, R. Schewski, M. Albrecht, Z. Galazka, W. Miller, J. Schwarzkopf, and A. Popp, Impact of chamber pressure and Si-doping on the surface morphology and electrical properties of homoepitaxial (100) β -Ga₂O₃ thin films grown by MOVPE, *Journal of Physics D: Applied Physics* **54**, 034003 (2020).
- [62] Y. Zhang, A. Neal, Z. Xia, C. Joishi, J. Johnson, Y. Zheng, S. Bajaj, M. Brenner, D. Dorsey, K. Chabak, G. Jessen, J. Hwang, S. Mou, J. Heremans, and S. Rajan, Demonstration of high mobility and quantum transport in modulation-doped β -(Al_xGa_{1-x})₂O₃/Ga₂O₃ heterostructures, *Applied Physics Letters* **112**, 173502 (2018).

ENDMATTER

Single crystal growth— Bulk single crystals were grown by the Czochralski method [13, 19, 20, 58, 59]. Substrates for homoepitaxy of 5x5 mm² were fabricated from the insulating Mg-compensation doped crystals.

Homoepitaxial film growth— Metal-organic vapour phase epitaxy was used for homo-epi film growth on (100) oriented substrates from single crystal growth. The substrates were off-oriented by 4° in [00-1] direction to avoid the formation of twin lamellae and to adjust the effective diffusion length to the terraces width with the aim to achieve step flow growth mode. The thin films were Si-doped using Tetraethylorthosilicate to enhance n-type conductivity. More details can be found elsewhere [17, 60, 61]. Atomic force microscope (AFM) measurements were performed on all thin films after growth to confirm step-flow growth by the surface topography and low RMS (RMS ≤ 1 nm), see [31].

Microlab for thermopower measurements— The microlabs consisting of Ti/Au (7 nm/35 nm) metal lines on the surface

of the films were manufactured by standard photolithography and magnetron sputtering. Deposited metal lines form a Schottky contact with the β -Ga₂O₃ and were contacted by attaching gold wire with indium at the contact-pads. Ohmic contacts were manufactured by wedge bonding with an Al/Si-wire (99%/1%). More details on the microlab and preparation can be found elsewhere [12, 28] and details for this study in [31]. To ensure the highest quality of the microlab, quality control of the structure was checked by a Raith PIONEER Two scanning electron microscope system.

Measurement techniques— All measurements were performed using standard source-meter-units (SMU). The measurement of the current-voltage characteristics for the van-der-Pauw, Hall and Seebeck measurements were performed with a Keithley 2450 SMU. The imprinting of the heating currents was done by a Keithley 2400 SMU. All measurements were performed in a CryoVac Konti-IT flow cryostat. The samples are in helium atmosphere at standard pressure. Van-der-Pauw-

and Hall-measurements are detailed in [31]

Models for the electrical properties– Application of fits of the charge neutrality equation and details of the scattering mechanisms that were used for determination of scattering rates are detailed in [31].

Thermopower measurements– For the determination of the Seebeck-coefficients measurements are carried out using a micro-lab on the chip [12, 57] consisting of metal line heaters, four-point metal line thermoemeters and ohmic contacts on these thermometers. An electrical current is imprinted into one of the line heaters close to the edge of the sample, which creates Joule heating. Thereon a temperature difference between the line heater and the edges of the sample is created which takes some time to become stable. The emerging thermovoltage can be measured at the points of the thermometers where ohmic contacts were prepared. At these points the temperature can be measured by the change of the resistance of

the four-point resistance of the thermometer lines. This procedure is done for several heating currents to calculate the Seebeck coefficient from the change of thermovoltage with temperature difference. This method has been shown to be successful [12, 57] and carried out for various bulk and thin film samples at different temperatures in a flow cryostat between $T = 50$ and 320 K. Below $T = 50$ K the thermal conductivity of β -Ga₂O₃ limits the measurement of the thermovoltage in this setup.

Models for the thermoelectric properties– The reduced chemical potential $\eta = (E_F - E_C)/k_B T$ was calculated using the formula of Nilsson [42], which is applicable to non-degenerate and degenerate semiconductors alike, and the calculation of the scattering parameter r using the analytic expressions for the momentum relaxation time τ , which were used to calculate the mobility, are detailed in [31].